Photon energy dependence of the perpendicular geometry magnetic circular dichroism in the 2p3p3p resonant photoemission from Ni

2000 J. Phys.: Condens. Matter 12 2123

(http://iopscience.iop.org/0953-8984/12/9/315)

J. Phys.: Condens. Matter **12** (2000) 2123–2133. Printed in the UK PII: S0953-8984(00)07644-X

Photon energy dependence of the perpendicular geometry magnetic circular dichroism in the 2p3p3p resonant photoemission from Ni

M Finazzi†, G Ghiringhelli, O Tjernberg and N B Brookes
European Synchrotron Radiation Facility, Boîte Postale 220, 38043 Grenoble Cédex, France

Received 9 September 1999

Abstract. The magnetic circular dichroism in the perpendicular geometry of the resonant 2p3p3p photoemission (PE) spectroscopy has been investigated in metallic Ni as a function of the photon energy across the Ni L_3 absorption edge. Within the experimental error bars, the photon energy dependence of the PE dichroism signal is the same as the one shown by the magnetic circular dichroism of the corresponding x-ray absorption (XMCD), obtained in the collinear geometry. This is attributed to the fact that, in metal Ni, the orbital $\langle L_z \rangle$ and dipolar $\langle T_z \rangle$ moments are smaller than the spin angular moment $\langle S_z \rangle$. The latter is the dominating term in both the expressions that give the integrated values of the PE dichroism or XMCD intensities. Although the respective photon energy dependence is very similar, the normalized PE dichroism intensity is a factor $\sim$5.6 smaller than the normalized XMCD signal, while only a factor $\sim$1.6 is expected from theoretical considerations. This factor is observed even below the L_3 threshold, thus we exclude that the small intensity of the perpendicular geometry dichroism in the Ni 2p3p3p resonant photoemission is due to fast relaxation processes in the intermediate state.

1. Introduction

Thanks to recent progress in insertion devices able to provide high intensity synchrotron radiation with polarization selectivity, light polarization dependent core level spectroscopy has become a very powerful tool to study the electronic and magnetic properties of condensed matter with site and shell selectivity. These techniques depend on the alignment of the valence band orbital and spin moments with the moments of the core hole created by the absorption of a circularly or linearly polarized photon. They have been widely applied to thin films and multilayer systems to study a wide variety of exotic magnetic behaviours such as oscillatory interlayer coupling, perpendicular magnetic anisotropy and giant magneto-resistance. These properties result from the interplay between spin–orbit interaction, hybridization, exchange coupling and crystal field. The determination of the orbital and spin parts of the total magnetic moment is thus a fundamental issue. In this respect, one of the most successful techniques is magnetic circular dichroism in x-ray absorption (XMCD). While normal x-ray absorption spectroscopy (XAS) measures the probability of creating a core hole (i.e. it measures its monopole moment), the integrated XMCD signals across the spin–orbit split edges depend on the first order polarization of the core hole, i.e. on the ground-state, shell- and site-projected orbital, spin and dipolar moments [1].

† New address: TASC–INFM, Elettra Synchrotron Light Source. S.S. 14-Km. 163.5, 34012 Basovizza, Trieste, Italy.

0953-8984/00/092123+11$30.00

In principle, higher-order magnetic and non-magnetic multipoles can be determined studying the angular dependence and the spin of the electrons emitted in the decay of the core hole [2]. In fact, in the resonant decay of the core hole following the absorption of polarized x-rays, the polarization of the core hole is transferred to the final state and to the electron leaving the sample [3–5]. The fact that the core hole has non-spherical symmetry is reflected by a non-isotropic angular distribution of the emitted electrons and their spin [2].

Magnetic circular dichroism in resonant photoemission (PE) spectroscopy consists in the difference between the resonant photoemission spectra obtained reversing the circular polarization of the x-rays impinging on a magnetized sample [6]. If the sample magnetization and the light wavevector are collinear, a large contribution to the PE dichroism is due to the light polarization dependent absorption cross-section at the origin of the XMCD effect [2, 3]. In the perpendicular geometry, i.e. when the sample magnetization and the wavevector of the circular light are orthogonal, a PE dichroism can still be observed, even if the absorption rate does not depend on the helicity of the photons [7]. This effect is the result of the intermediate-state core hole carrying a quadrupole moment. Its resonant recombination affects in a different way the angular distribution of the various components of the PE spectrum. The symmetry between the two mirror conditions obtained by reversing the polarization of the light is broken when the detection of the emitted electrons is performed with angular resolution along an axis non-collinear with the photon beam or the sample magnetization (but not when the magnetization is perpendicular to the plane of measurement) [2, 7]. The same mechanism is also active when the intermediate-state core hole decays in a *radiative* way and the outgoing photon is detected within a small solid angle in a resonant Raman scattering (RRS) experiment. An example of RRS magnetic circular dichroism in the perpendicular geometry has been reported very recently for the $3d^n \rightarrow 2p^5 3d^{n+1} \rightarrow 3s^1 3d^{n+1}$ scattering of metallic Co and of Ni in $NiFe_2O_4$ [8].

In the present paper we investigate the behaviour of the 2p3p3p resonant photoemission magnetic circular dichroism as the photon energy is scanned across the Ni L_3 absorption edge of metallic nickel. The aim is to understand what information can be extracted from the photon energy dependence of the 2p3p3p dichroism in Ni. The interest of studying Ni consists in the fact that Ni is often considered as a prototype system in the 3d transition metal series regarding strong correlations in the ground, core- and valence-excited states. These many-body effects directly correlate to satellite features in the spectra, which are a sign of configuration interaction [9]. Examples are the large satellite visible in the XAS spectrum at ∼6 eV above the L_3 maximum and the XMCD satellite at ∼4 eV [10]. Recently, core-excited states and their decay processes in metal Ni [3, 11, 12] or NiO [13–15] have also been studied using resonant photoemission spectroscopy.

2. Experiment

The resonant photoemission data were collected at the Dragon beam line ID12B at the European Synchrotron Radiation Facility (ESRF) [16], using the circularly polarized light emitted by the helical undulator Helios I [17]. The measured rate of circular polarization of the photons at the $L_{2,3}$ absorption edges of Ni (850–870 eV) was ∼85% [18]. The photon energy resolution was estimated to be ∼350 meV. The energy distribution of the photoelectrons was measured using a commercial hemispherical analyser (PHI model 3057, mean diameter 279.4 mm) with multichannel detection. The bandwidth of the analyser was set to ∼500 meV, while its acceptance angle was ±20°. The axis of the analyser was at an angle of 60° with respect to the direction of propagation of the light. The samples were Ni thin films grown *in situ*

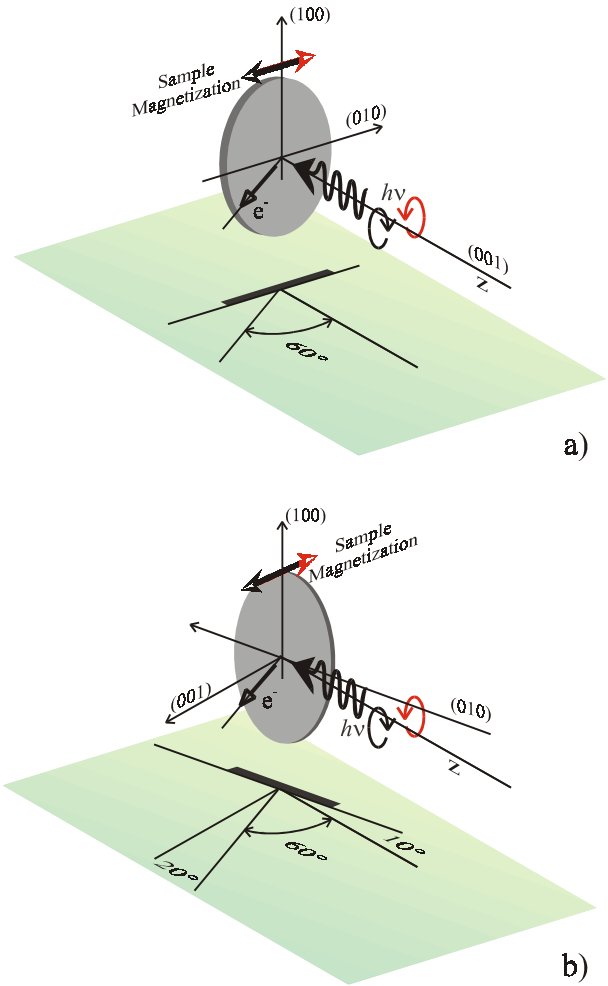

Figure 1. The two experimental setups for the perpendicular geometry PE dichroism experiment: (a) sample magnetized in plane and normal light incidence; (b) sample magnetized out of plane and grazing light incidence.

on a Cu(001) single-crystal surface by e^--beam evaporation from a pure (4 N) nickel rod. The copper substrate was cleaned by successive cycles of argon sputtering and annealing. Two geometries have been studied (see figure 1). In Ni films thicker than ∼60 ML the easy magnetization axis is in plane. In this case, the photon wavevector was set perpendicular to the surface. A grazing light incidence geometry had been chosen for samples thinner than ∼60 ML, for which the easy axis is out of plane. The Ni films were magnetized at remanence by a pulsed magnetic field (amplitude on the sample: 200 mT; length: 5 ms) in the plane defined by the axis of the analyser and the direction of propagation of the light. The PE dichroism data were collected reversing the sample magnetization or the polarization of the light between two successive acquisitions. All the data presented in this paper were recorded at room temperature.

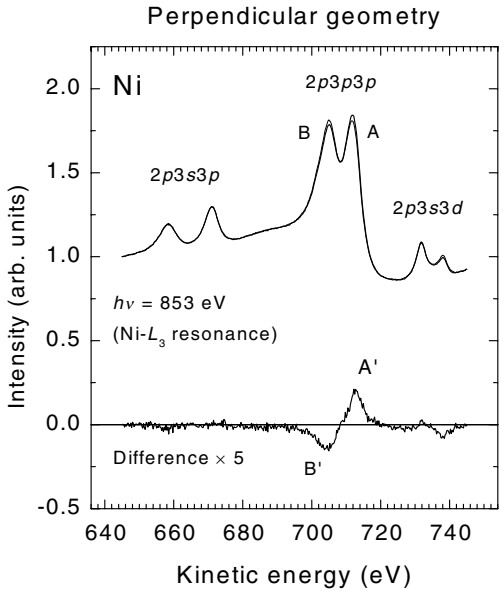

Figure 2. Resonant photoemission spectra of Ni metal collected at $h\nu = 853$ eV and the difference spectra produced by reversing the sample magnetization or the circular polarization of the light in perpendicular geometry. The spectra have been arbitrarily normalized to unity at a kinetic energy of 645 eV. The difference between the normalized spectra is shown multiplied by five.

3. Results

Figure 2 shows electron energy distribution spectra collected with opposite combinations of light circular polarization and direction of magnetic field. They have been measured at $h\nu = 853$ eV, corresponding to the maximum of the Ni L_3 absorption spectrum on a sample magnetized out of plane. The kinetic energy range covers the region of the 2p3s3p ($L_3M_1M_{2,3}$) and 2p3p3p ($L_3M_{2,3}M_{2,3}$) resonant PE peaks, and of the 3s photoemission line at resonance with the 2p3s3d ($L_3M_1M_{4,5}$) line. The spectra have been normalized to unity at the kinetic energy of 645 eV to compensate possible intensity variations in the photon flux between two successive acquisitions and to remove any residual dichroism in absorption induced by the non perfect orthogonality between the light wavevector and the sample magnetization. The exchange interaction splits the photoemission lines into two peaks depending on the relative orientation of the spin of the two final state holes. In the 2p3p3p manifold peak A has ^{3}P symmetry, while peak B results from the superposition of singlets of ^{1}S and ^{1}D symmetry [7].

The difference between the two normalized spectra, corresponding to the PE dichroism in normal geometry, is plotted multiplied by five. Its intensity is close to the one reported in the literature [7]. At correspondence with the 2p3p3p lines, the difference shows the typical negative–positive line shape, since triplet and singlet final states give opposite contributions to the dichroism signal [7]. Note that no dichroism is observed at correspondence with the 2p3s3p manifold. This is related to the fact that the distribution of the charge of a 3s core hole in the final state is spherical. The small magnetic signal visible at correspondence with the 2p3s3d resonant photoemission is only observed in the geometry indicated in the bottom part of figure 1, and disappears completely when the sample magnetization and the light helicity are really perpendicular as in the case described in figure 1(a). We believe that, in spite of the

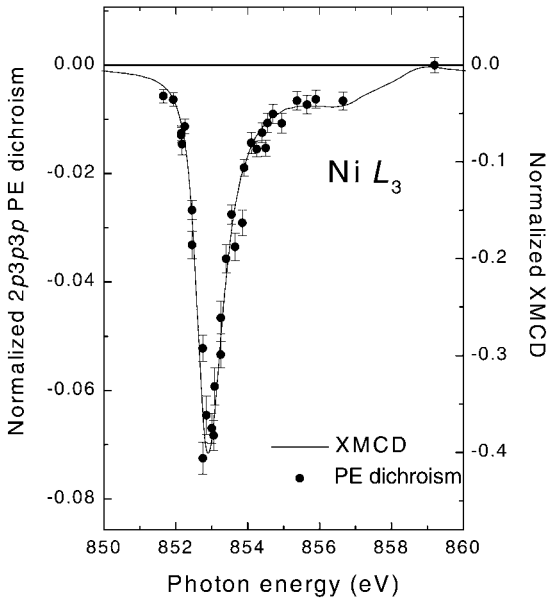

Figure 3. Photon energy dependence of the perpendicular geometry PE dichroism and XMCD, the latter collected with collinear sample magnetization and light helicity. The PE dichroism is normalized to the magnitude of the light polarization averaged PE spectrum at the L_3 absorption maximum ($h\nu = 853$ eV). The XMCD signal is normalized to the light polarization averaged absorption at the same energy. Both the PE dichroism and the XMCD signals have also been rescaled to take into account the incomplete circular polarization of the light (∼85%).

fact that the 3s hole is isotropic, the dichroism on the 2p3s3d peaks is induced by configuration interaction with the 2p3p3p lines [2].

Figure 3 shows the photon energy dependence of the intensity of the PE dichroism normalized to the photon flux. Note that in figure 2 the final-state lifetime broadening of the 2p3p3p features is comparable with the energy separation between the singlet and the triplet states. Since they give opposite contributions in the difference spectra, this leads to a partial cancellation of the dichroic effect. In fact, the sum of a positive and a negative peak, weakly separated in energy, gives a curve where both the peak height and the integral of the absolute value are reduced. To avoid this complication and in order to make direct comparison with the sum rules of [7], we have fitted the features in the difference spectra with Lorentzians, allowing the tails of the opposite-sign fitting curves to overlap. Then, as a measure of the intensity of the PE dichroism, we take for each photon energy the sum of the absolute values (multiplied by -1 in figure 3) of the areas of the Lorentzians fitting the 2p3p3p difference spectrum. In this way we also minimize the consequences of transferring spectral weight between the positive and the negative PE dichroism features induced by variations in the background of PE spectra collected with opposite polarization. The PE dichroism has also been rescaled to the area of the polarization averaged 2p3p3p PE spectrum collected at $h\nu = 853$ eV. In figure 3, we plot data obtained with both the geometries described in figure 1. The magnitude of the PE dichroism signals measured on the film showing an out-of-plane easy magnetization axis (figure 1(b)) has been scaled in order to correct the different magnetization of the sample. We have measured the PE peaks for photon energies up to $h\nu = 885.4$ eV, corresponding to ∼15 eV above the L_2 threshold, but a dichroism signal is visible only for photon energies less than 856.5 eV (about 3.5 eV above L_3). This is expected since, at the L_2 edge, the $2p_{1/2}$ core hole does not carry

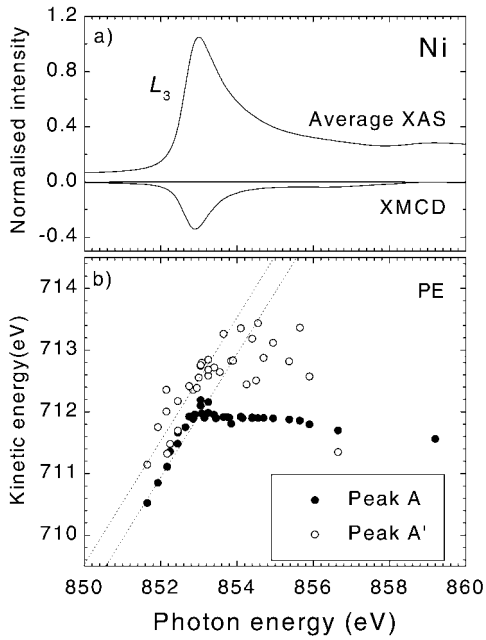

Figure 4. (a) XMCD and light polarization averaged XAS spectra. (b) Kinetic energy position against photon energy of peak A (see the resonant photoemission spectra of figure 2) and of peak A′ (PE dichroism spectrum in figure 2). The horizontal line at K.E. = 711.9 eV indicates the kinetic energy of peak A at $h\nu = 885.4$ eV (i.e. above the Ni L_2 edge). The diagonal dashed lines correspond to constant binding energy points.

any quadrupole moment, and the intermediate states with a $2p_{3/2}$ core hole become more and more isotropic as the photon energy is increased well above the L_3 resonance.

Figure 3 also shows the XMCD spectrum collected with collinear sample magnetization and light helicity in the total electron yield mode measuring the sample drain current. The XMCD signal has been normalized to the light polarization averaged absorption at $h\nu = 853$ eV, corresponding to the L_3 edge maximum. It is interesting to notice that, within the experimental error bars ($\pm 4\%$ at $h\nu = 853$ eV), the PE dichroism and XMCD normalized signals follow the same photon energy dependence. The PE dichroism also reproduces fairly well the satellite at $\sim$4 eV above the L_3 maximum. The main difference is that the PE dichroism magnitude is about 5.6 times smaller than the XMCD. This factor will be discussed below.

The kinetic energy position of peak A of the average photoemission spectrum and of the corresponding peak A′ of the PE dichroism (see figure 2) are shown in figure 4 as a function of the photon energy. For $h\nu < 853$ eV, we observe peak A at constant binding energy. This is typical of the radiationless resonant Raman emission, which is obtained when the photon energy is set below an absorption threshold [19]. For photon energies above the L_3 maximum, peak A is observed at constant kinetic energy, as expected when the photoelectron is excited into a continuum of states [19]. Even if the data concerning the PE dichroism data are more scattered, peak A′ basically follows the same photon energy dependence of peak A, apart from an offset of $\sim$1 eV towards higher kinetic energies both in the constant-kinetic- and in the constant-binding-energy regime. According to the theory of inelastic scattering, in the region where A and A′ are detected at constant binding energy (Raman behaviour) the photon absorption and electron emission cannot be considered as independent processes, but have to be viewed using

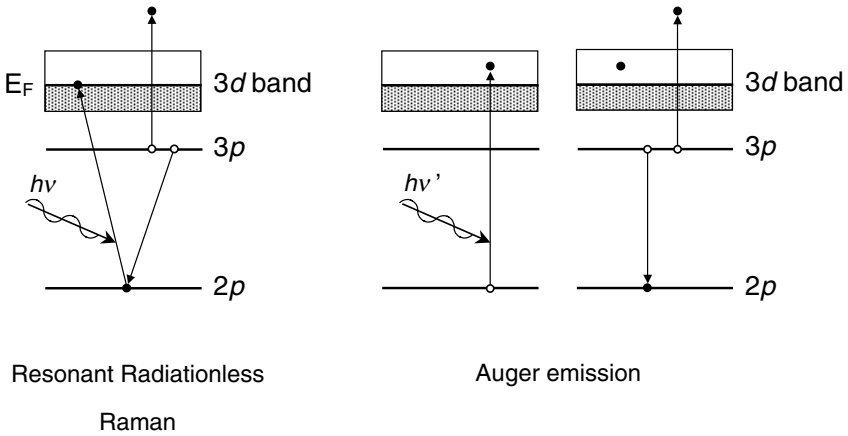

Figure 5. Schematic representation of the radiationless Raman and Auger 2p3p3p ($L_3M_{2,3}M_{2,3}$) emission.

a second-order, single-step perturbation model (see diagram in figure 5) [19]. In this region, the photoelectron is excited into the lowest lying empty valence band state and the extra energy needed for this transition is subtracted from the emitted electron, which is detected at constant binding energy. At photon energies above threshold, the photoelectron can be excited into any accessible conduction band state. In this way, normal Auger behaviour is retrieved, with peaks being detected at constant kinetic energy. Although the process described above, giving rise to the Raman regime is still allowed, both the PE dichroism and the polarization averaged PE signals are dominated by the Auger emission, as shown by the behaviour of the peak position in figure 4.

4. Discussion

The photon energy dependence of the photoemission and PE dichroism peaks plotted in figure 4 demonstrates that above threshold the absorption and decay steps can be separated and, hence, that the photoelectron excited into the intermediate state acts only as a spectator of the core-hole decay. According to [2], this allows us to express the normalized L_3 PE dichroism intensity in the perpendicular geometry with the expression [7]

$$\frac{J^{diff}}{J^{ave}}(\text{PE dichroism}) \sim 3\frac{J^1}{J^0} = 3\frac{(\frac{3}{5}\underline{w}^{101} + \underline{w}^{011} + \frac{1}{5}\underline{w}^{211} - \frac{3}{5}\underline{w}^{303} - \frac{6}{5}\underline{w}^{213})}{(2\underline{w}^{000} + \underline{w}^{110})} \times \frac{B^2_{3/2}(LS)}{B^0_{3/2}(LS)}(\boldsymbol{P}\cdot\boldsymbol{\varepsilon})(\boldsymbol{\varepsilon}\cdot\boldsymbol{M}). \quad (1)$$

In this equation, J^{ave} is the integral across the L_3 edge of the PE intensity averaged upon circular light polarization and sample magnetization reversal, while J^0 and $J^1 = J^{diff}$ represent respectively the L_3 integrated isotropic PE intensity and PE dichroism [20]. The terms $\underline{w}^{xyz}$ are expectation values of the moments (with $\boldsymbol{M}$ as quantization axis) of the empty levels of the ground state. The xyz indices are a systematic way to indicate the kind of moment involved [21]. For a d shell: $\underline{w}^{011} = 2\langle S_z\rangle$, $\underline{w}^{101} = 1/2\langle L_z\rangle$ and $\underline{w}^{211} = 7/2\langle T_z\rangle$, with $\langle S_z\rangle$, $\langle L_z\rangle$ and $\langle T_z\rangle$ being respectively the 3d spin, orbital and dipolar ground state angular moments, while, according to [7], $\underline{w}^{213} \approx \underline{w}^{211}$ and $\underline{w}^{303} \approx 0$. The quantization axis z is taken parallel to the

sample magnetization. The coefficients $B_j^r(LS)$ depend on the probability that a core hole with moment r decays into the final state LS. For 2p3p3p dichroism, $B^2_{3/2}(^3\mathrm{P})/B^0_{3/2}(^3\mathrm{P}) = 0.5$ and $[B^2_{3/2}(^1\mathrm{D}) + B^2_{3/2}(^1\mathrm{S})]/[B^0_{3/2}(^1\mathrm{D}) + B^0_{3/2}(^1\mathrm{S})] = -0.49$ [7]. The last term in equation (1), containing the light helicity vector $\boldsymbol{P}$, the sample magnetization $\boldsymbol{M}$ and the unit vector $\boldsymbol{\varepsilon}$ pointing in the direction of the electron analyser, gives the angle dependence of the process. Note that, in metallic Ni, the dominating contribution to the numerator of the right term of equation (1) is $\underline{w}^{011}$. In fact, using the experimental values for $\underline{w}^{xyz}$ that can be deduced from the literature for bulk Ni [7], or the theoretical values of the moments calculated for the Ni(100) surface [22], we find that disregarding in the numerator all the moments except $\underline{w}^{011}$ only leads to an error of $\sim$5%.

The L_3 XMCD normalized intensity depends on the $\underline{w}^{xyz}$ moments through the following expression [23]:

$$\frac{J^{diff}}{J^{ave}}(\mathrm{XMCD}) \sim 3\frac{J^1}{J^0} = 3\frac{(2\underline{w}^{101} + \frac{1}{3}\underline{w}^{011} + \frac{2}{3}\underline{w}^{211})}{(2\underline{w}^{000} + \underline{w}^{110})}(\boldsymbol{P}\cdot\boldsymbol{M}). \tag{2}$$

Similarly to equation (1), J^0 and $J^1 = J^{diff}$ represent respectively the isotropic x-ray absorption and the XMCD intensity integrated across the L_3 edge. J^{ave} is the integral of the light polarization and sample magnetization averaged XAS spectrum [20].

In this case, the error introduced when only the $\underline{w}^{011}$ term is retained is slightly higher than for PE dichroism, being equal to $\sim$10% for bulk metal Ni. The error is, however, still small, such that the $\langle T_z\rangle$ term can be neglected in the application of the XMCD spin dependent sum rule [1] to 3d transition metals [24]. Note that, in late 3d systems, both equations (1) and (2) are subjected to an intrinsic error of $\sim$5%, which is due to the spin–orbit splitting of the $L_{2,3}$ edges not being large enough to prevent the mixing between the $2p_{3/2}$ and $2p_{1/2}$ states induced by the Coulomb interactions acting on the core hole [1]. From these considerations we see that both XMCD and perpendicular geometry PE dichroism at the L_3 edge of Ni are essentially sensitive to just the spin moment of the 3d states.

Conserving only the $\underline{w}^{011}$ moment in the numerator of equations (1) and (2), we obtain that, in the geometry of our experiment, the ratio between the XMCD and PE dichroism relative intensities integrated across the L_3 edge should be about 1.6. Note that, applying the above assumption, this ratio no longer depends on any $\underline{w}^{xyz}$ multipole. The value of the ratio expected from equations (1) and (2) is $\sim$3.5 times smaller than the one that we observe (which is $\sim$5.6), in good agreement with the findings of [7], where the experimental PE dichroism intensity is about a factor of three smaller than the theoretical value. It is interesting to remark that the perpendicular geometry magnetic circular dichroism measured on the RSS spectrum of metallic Co is about a factor of two smaller than the value extrapolated from the RSS dichroism of Ni in $NiFe_2O_4$, which is, in contrast, in close agreement with theoretical expectations based on an ionic model [8].

An important difference between PE dichroism and XMCD is represented by the surface sensitivity of these techniques. Electrons with a kinetic energy of about 700 eV, such as the ones emitted by the resonant 2p3p3p photoemission process in Ni, have an escape depth in metals of the order of 5–10 Å [25]. On the other hand, the probing depth of XAS is 25 ± 3 Å when the absorption spectrum is collected measuring the yield of secondary electrons at the Ni $L_{2,3}$ edge [26]. This does not seem to explain the low intensity of the PE dichroism signal, since the Ni surface moment is expected to be $\sim$15% larger than in the volume [22]. Moreover, with an escape depth of 5–10 Å, a significant part of the PE dichroism signal comes from a region of the sample that can be considered as representative of the bulk.

A mechanism that could explain the low value of the PE dichroism intensity is the presence of fast relaxation processes that destroy the moment created in the intermediate

state after the absorption of a circularly polarized photon. The effects of such processes are however strongly reduced for excitations below threshold. In fact, as explained above, in these conditions the photoelectron is excited into the lowest accessible level and no further relaxation of the intermediate state is thus possible before the recombination of the core hole. However, the ratio between the PE dichroism and XMCD signals remains the same below as well as above the L_3 threshold, thus excluding a significant intervention of fast relaxation processes. Nevertheless, it might be argued that, below threshold, the approximation consisting in assuming the photoelectron as a spectator of the Auger decay of the core hole is no longer valid [19], and, therefore, that equation (1) cannot be applied. Hence, no connection between the intensity of the PE dichroism below and above threshold should be expected. Actually, equation (1) also holds for the radiationless Raman case if the dipole allowed intermediate states that decay into the same final state all lie within an energy region smaller than the intermediate-state lifetime broadening [2]. If this condition is not fulfilled, equation (1) contains cross-terms coupling the absorption and emission steps that are absent in reality. In metallic Ni, electron correlation in the 3d band induces a large satellite in the XAS spectrum at ∼6 eV above the L_3 edge [9]. Thus, 3d spectral weight is spread over a photon energy region in the L_3 absorption spectrum which is much larger than the 2p lifetime broadening (∼2 eV). For this reason, equation (1) is not strictly valid below threshold. Note, however, that the contribution of the extra terms in equation (1) due to the satellite states is proportional to the intensity of the satellite itself. Since the latter is weak compared to the main absorption resonance, small deviations from equation (1) are expected, which cannot be held responsible of the large mismatch between the theoretical and experimental PE dichroism intensity.

Equations (1) and (2) give the values of L_3 integrated signals. The integration is necessary to eliminate the dependence of the matrix elements on the intermediate state in PE or on the final state in XAS and to relate the experimental data to ground state properties (the $\underline{w}^{xyz}$ multipoles) [2]. The condition that both XMCD and PE dichroism essentially depend on the same quantity, namely $\underline{w}^{011}$, is not sufficient to justify the same photon energy dependence of both the PE dichroism and XMCD signals. The same $h\nu$ dependence is obtained if each state excited after the absorption of a photon gives contributions to the XMCD signal and the PE dichroism always in the same proportions. These contributions depend on the multipoles of the photoelectron excited in the in the valence band of the system. In particular they will be proportional to the density of states, which relates to $\underline{w}^{000}$. Thus, the same photon energy dependence might be expected if in all the photoelectron states the only non-vanishing multipoles are $\underline{w}^{011}$ and $\underline{w}^{000}$. For this, the conditions $|\underline{w}^{011}| \gg |\underline{w}^{101}|$ and $|\underline{w}^{011}| \gg |\underline{w}^{211}|$ must hold not only for the $\underline{w}^{xyz}$ moments integrated over all the empty 3d levels, but also for their energy distributions across the 3d conduction band. In 3d transition metals, the first condition is certainly verified, since the spin–orbit interaction is small compared to the crystal field, which quenches the orbital moment of the d electrons. Calculations for the Ni(100) surface, where the orbital moment is expected to be larger than in the bulk, $\langle L_z \rangle$ always remains about a factor 10 smaller than S_z independently from the energy of the empty states [22]. On the other hand, the energy distributions of $\underline{w}^{011}$ and $\underline{w}^{211}$ calculated for the Ni(100) surface show that $2\langle S \rangle_z$ and $7\langle T \rangle_z$ assume comparable values for all the energies above the Fermi level [22]. Although the high relative value of $\underline{w}^{211}$ can be neglected in equation (1), it leads to an error that can be as high as 100% if omitted in equation (2). However, XMCD is not a surface sensitive technique, and in the bulk the $\langle T_z \rangle$ term is strongly reduced. In fact, in the bulk, the cubic symmetry of the lattice limits the anisotropy of the spin density distribution around the absorbing atom and, hence, it reduces the expectation value of T_z. According to [22], the $\langle T_z \rangle$ moment in the bulk is a factor ∼3 smaller than at the surface. Moreover, $\langle T_z \rangle$ is a rapidly oscillating function over the d band [22]. The photon energy dependence of the PE peaks is given by a Kramers–

Heisenberg-type formula, which includes a convolution between the valence band and the Lorentzian describing the finite lifetime of the 2p core hole. Such a convolution will smear out the energy dependence of $\langle T_z \rangle$, further reducing its contribution to the PE dichroism. From the theoretical energy distributions of $2\langle S \rangle_z$ and $7\langle T \rangle_z$ given in [22] it might be concluded that the bulk value of $\underline{w}^{211}$ is never more than $\sim$20% the value of $\underline{w}^{011}$ for any energy above E_F. This means that the XMCD signal should track the one of the PE dichroism (where only $\underline{w}^{011}$ gives a significant contribution) with a precision better than $\sim$20%. Apart from the scaling factor between the XMCD and PE dichroism intensities that still remains unexplained, we find that our experimental data fall within this range. The fact that at the Ni L_2 edge the PE dichroism vanishes while an XMCD signal is still observed is not in contradiction with the explanation given above. In fact, the ratio between XMCD and PE dichroism should depend on the C_j^{xyzar} coefficients described in [2], which depend on the absorption edge.

5. Conclusions

We have investigated the photon energy dependence of the magnetic circular dichroism of the 2p3p3p photoemission in the perpendicular geometry while the energy of the incoming photon was scanned across the Ni L_3 absorption threshold. Within the experimental error bars, the photon energy dependence of the PE dichroism is the same as the one followed by XMCD in collinear geometry. This is attributed to the fact that, in Ni as well as in other magnetic 3d metals, the distribution of the $\langle T_z \rangle$ and $\langle L_z \rangle$ moments in the conduction band is much smaller than the one of the spin $\langle S_z \rangle$. As a consequence, only the terms depending on $\underline{w}^{011}$ can be retained in both the equations giving the intensity of XMCD and PE dichroism respectively. For this reason, a different photon energy dependence of the PE dichroism and XMCD signals is expected for more localized compounds, such as transition metal oxides or rare earths, or for low dimensionality systems such thin films, multilayers or clusters. In these cases, at variance from bulk 3d metals, the $\langle L_z \rangle$ and $\langle T_z \rangle$ moments cannot be neglected compared to $\langle S_z \rangle$, as demonstrated by the important role they play in determining the magnetic properties of these systems.

The comparison of the PE dichroism and XMCD relative intensities show that the PE dichroism is a factor $\sim$3.5 smaller than the theoretical value. We do not have a clear explanation for this finding, but we can exclude the presence of fast relaxation processes that could lead to the reduction of the moment of the PE intermediate state. In fact, the intensity of the PE dichroism remains small even below the Ni L_3 edge, where the effects of intermediate-state relaxation should be reduced.

Acknowledgments

We would like to acknowledge Maurizio Sacchi for fruitful discussion and Kenneth Larsson for his excellent technical assistance.

References

[1] Carra P, Thole B T, Altarelli M and Wang X 1993 *Phys. Rev. Lett.* **70** 694
[2] van der Laan G and Thole B T 1995 *Phys. Rev.* B **52** 15 355
van der Laan G and Thole B T 1995 *J. Phys.: Condens. Matter* **7** 9947
[3] Tjeng L H, Chen C T, Rudolf P, Meigs G, van der Laan G and Thole B T 1993 *Phys. Rev.* B **48** 13 378
[4] Tjeng L H *et al* 1997 *Phys. Rev. Lett.* **78** 1126
[5] Sinkovic B *et al* 1998 *Phys. Rev. Lett.* **79** 3510

van der Laan G 1998 *Phys. Rev. Lett.* **81** 733

[6] In the dipolar approximation, reversing the light helicity with fixed sample magnetization gives the same result as reversing the sample magnetization with fixed light helicity. For dichroism in photoemission see [7], while for XMCD see Brouder Ch and Kappler J-P 1997 *Synchrotron Radiation and Magnetism* ed E Beaurepaire, B Carrière and J P Kappler (Les Ulis: Edition de Physique) p 19

[7] Thole B T, Dürr H A and van der Laan G 1995 *Phys. Rev. Lett.* **74** 2371

[8] Braicovich L *et al* 1999 *Phys. Rev. Lett.* **82** 1566

[9] See, for instance, S. Hüfner in *Photoemission in Solids II* ed L Ley and M Cardona (Berlin: Springer) p 173

[10] Chen C T, Smith N V and Sette F 1991 *Phys. Rev.* B **43** 8771

[11] Weinelt M *et al* 1997 *Phys. Rev. Lett.* **78** 967

[12] Magnuson M, Wassdahl N, Nilsson A, Föhlisch A, Nordgren J and Mårtensson N 1998 *Phys. Rev.* B **58** 3677

[13] Nakamura M, Takata Y and Kosugi N 1996 *J. Electron. Spectrosc.* **78** 115

[14] Tjernberg O, Söderholm S, Karlsson U O, Chiaia G, Quarford M, Nylén H and Lindau I 1996 *Phys. Rev.* B **53** 10 372

[15] Finazzi M, Brookes N B and de Groot F M F 1999 *Phys. Rev.* B **59** 9933

[16] Goulon J, Brookes N B, Gauthier C, Goedkoop J B, Goulon-Ginet C, Hagelstein M and Rogalev A 1995 *Physica* B **208/209** 199

[17] Elleaume P 1994 *J. Synchrotron Radiat.* **1** 19

[18] Drescher M, Snell G, Kleinberg U, Stock H-J, Müller N, Heinzmann U and Brookes N B 1997 *Rev. Sci. Instrum.* **68** 1939

[19] Åberg T and Crasemann B 1994 *Resonant Anomalous X-ray Scattering* ed G Materlik, C J Sparks and K Fischer (Amsterdam: Elsevier) p 431

[20] For both XAS and PE, $6J^{ave} - 2J^0 = J^2$, with $J^2 = L_3$ integrated linear dichroism. In 3d transition metals, the XAS linear dichroism is typically a factor 40 to 100 smaller than the light polarization averaged spectrum (see Schwickert M M, Guo G Y, Tomaz M A, O'Brien W L and Harp G R 1998 *Phys. Rev.* B **58** R4289). For this reason, we expect that for XAS the approximation $J^{ave} \sim J^0/3$ should be valid within an error smaller than 1%. From [2] we obtain that the ratio J^2/J^0 in photoemission should be of the same order of magnitude as in XAS. Therefore, we feel confident that the approximation $J^{ave} \sim J^0/3$ can be safely applied to PE as well.

[21] Thole B T, van der Laan G and Fabrizio M 1994 *Phys. Rev.* B **50** 11 466

[22] Wu R and Freeman A J 1994 *Phys. Rev. Lett.* **73** 1994
Wu R, Wang D and Freeman A J 1994 *J. Magn. Magn. Mater.* **132** 103

[23] van der Laan G 1998 *Phys. Rev.* B **57** 112

[24] Chen C T, Idzerda Y U, Lin H-J, Smith N V, Meis G, Chaban E, Ho G H, Pellegrin E and Sette F 1995 *Phys. Rev. Lett.* **75** 152

[25] Matthew J A D, Jackson A R and El-Gomati M M 1997 *J. Electron Spectrosc.* **85** 205

[26] Nakajima R, Stöhr J and Idzerda Y U 1999 *Phys. Rev.* B **59** 6421